CHEMISTRY
AN ASIAN JOURNAL
ACES
FULL PAPER

DOI: 10.1002/asia.201300626

Facile Solution Synthesis and Photoelectric Properties of Monolithic Tin(II) Sulfide Nanobelt Arrays

Xing Zhang,[a] Long Yang,[b] Yan Jiang,[a] Bin-Bin Yu,[a] Yu-Gang Zou,[a] Ying Fang,[b] Jin-Song Hu,*[a] and Li-Jun Wan*[a]

Dedicated to Professor Chun-Li Bai on the occasion of his 60th birthday

Abstract: The tremendous future energy demand and environmental concerns prompt the lasting search for new materials for low-cost and high-efficiency solar cells. SnS, as a low-cost, earth-abundant, and environmentally friendly material with proper band gap and absorption coefficient, has received attention as a potential candidate for solar absorber, but it is still under-developed due to insufficient conversion efficiency. Fabricating SnS nanostructured films for solar cell design could be effective to boost photovoltaic performance and pave the way for applications in photovoltaics. Herein, a facile surfactant-free solution-based approach has been developed to prepare monolithic SnS nanostructured films directly on tin foil substrate. The morphologies of nanostructured films could be tuned from well-defined orthorhombic SnS nanobelt arrays to nanorods, nanosheets, or nanoflakes by simply changing the ratio of used solvents. The photoelectric response and electronic transportation properties of SnS nanobelts were investigated by fabricating single-nanobelt-based nanodevices. The SnS nanobelt exhibited a fast and reliable photoresponse even at illumination intensity as weak as $0.103\,mW\,cm^{-2}$. The measurements on SnS FET devices also indicated that the synthesized SnS nanobelts demonstrated a hole mobility as high as $12.33\,cm^2\,V^{-1}\,s^{-1}$. These results reveal that the reported approach for preparing monolithic SnS nanostructured films could be useful to further develop SnS as an alternative material for low-cost solar cells and electronic devices.

Keywords: nanostructures · photophysics · solar cells · sulfur · tin

Introduction

With the tremendous energy demand for human activities and lasting environmental concerns from traditional energy sources, the exploration of clean energy sources is of great urgency, among which solar energy is given priority over all alternatives owing to its abundance and environmental friendliness. Although substantial progress has been made in silicon, copper indium gallium selenide (CIGS), dye-sensitized, and organic solar cells, scientists never stop seeking materials for next-generation low-cost and high-efficiency thin-film solar cells. Those based on earth-abundant elements are especially attractive from the viewpoint of commercial viability and their potential as replacements for traditional carbon-based energy sources in terms of both huge demand in terawatt scale and practicable cost of electricity generation in price per kWh. In the past decades, several binary material options, including SnS, FeS_2, Cu_2S, and Cu_2O, had been explored and shown attractive capabilities of light absorption and photoelectric conversion, but research progress was severely hindered by very low conversion efficiency and device stability.[1] The emergence and rapid development of modern nanotechnologies may offer a chance for the renaissance of these materials.[2] Therefore, the fabrication of nanostructures of the above-mentioned materials for photovoltaics would be very attractive and important.

Tin(II) sulfide, as a p-type semiconductor with direct and indirect band gaps of 1.2–1.5 eV and 1.0–1.2 eV, respectively,[3] has received considerable attention as a potential candidate for solar absorber. It is composed of low-cost, earth-abundant, and environmentally friendly elements, and it is a binary material, thus its solution-based thin-film deposition requires consideration of only two elements, which makes chemical strategies much less complex. To date, most of studies focused on the synthesis of SnS nanomaterials, such as quantum dots,[4] nanocrystals,[5] one dimensional (1D) nanostructures,[3a,6] and nanosheets,[7] rather than thin-

[a] X. Zhang, Y. Jiang, B.-B. Yu, Y.-G. Zou, Prof. J.-S. Hu, Prof. L.-J. Wan
Beijing National Laboratory for Molecular Sciences
CAS Key Laboratory of Molecular Nanostructure and Nanotechnology
Institute of Chemistry, Chinese Academy of Sciences (CAS)
Beijing 100190 (P.R. China)
Fax: (+86) 10-82613929
E-mail: hujs@iccas.ac.cn
wanlijun@iccas.ac.cn

[b] L. Yang, Prof. Y. Fang
National Center for Nanoscience and Technology
Beijing, 100190 (P. R. China)

Supporting information for this article is available on the WWW under http://dx.doi.org/10.1002/asia.201300626.

film development. There are a few reports of photovoltaic devices incorporating SnS with low efficiencies of less than 1%.[8] Further intensive investigation on better strategies for solution deposition of this promising absorber will be required before it contributes to practicable solar cells. Moreover, it was recently shown that the conversion efficiency of photovoltaic devices can be significantly enhanced by nanostructuring the thin-film light-absorber layer to improve light absorption and increase p–n junction area.[9] Especially, fabrication of 1D nanostructure arrays has been demonstrated as an effective way to enhance light absorption by scattering and light trapping and thus ameliorate the conversion efficiency of solar cells.[10] Accordingly, the development of solution-based routes to produce SnS nanostructures,[11] especially to directly produce monolithic nanostructured films, would be significant and highly desirable to explore their potential in photovoltaics in view of low-cost and less complex production processes and possible improvement for conversion efficiency.

Herein, a facile surfactant-free solution-based approach has been developed to prepare a monolithic SnS nanostructured film composed of well-defined orthorhombic SnS nanobelt arrays. The morphologies of SnS nanostructured films can be easily controlled by simply changing the reaction conditions. As a demonstration of this material for potential application in photovoltaics and electronic applications, we investigated photoelectric response and electric properties of SnS nanobelts by fabricating nanodevices based on single SnS nanobelts. This approach was expected to provide a facile way to explore SnS and other sulfide nanostructured thin-film solar cells as well as the corresponding hybrid solar cells, although the devices based on these nanostructures need to be investigated further.

Abstract in Chinese:

SnS 是一种具有合适带宽和吸光系数的低成本、含量丰富和环境友好的材料，因此是低成本太阳能电池理想的吸收层材料之一，但是基于这种材料的太阳能电池效率仍然很低。构筑 SnS 纳米结构化薄膜是提高其光伏性能从而促进其在光伏领域应用的有效途径之一。本文发展了一种简单的溶液相合成技术,直接在金属锡箔表面构筑了由单晶 SnS 一维纳米带阵列构成的纳米结构化薄膜。研究发现薄膜的结构可以通过简单地改变混合溶剂的比例来调节。通过构筑和测试基于单根 SnS 纳米带的纳米器件，表明这种 SnS 纳米带即使在弱光下也能表现出优异的光电响应，并且其空穴迁移率高达 12.33 $cm^2\ V^{-1}\ s^{-1}$。这些研究结果有助于进一步开发 SnS 作为低成本、环境友好的太阳能电池吸收层材料。

Results and Discussion

Tin(II) sulfide nanostructures were prepared under simple solvothermal conditions with tin foil and sulfur powder as source materials and a mixture of octylamine and octanol as solvent. It was found that well-defined nanobelt arrays could be obtained when using octylamine and octanol at volume ratio of 1:1. Figure 1a is a typical photograph of the synthesized product, which shows that the whole area of the silver-white tin foil turned dark brown after reaction. The composition and crystal structure of the product were first investigated by X-ray diffraction (XRD). Figure 1b presents a typical XRD pattern of the product and a reference XRD pattern of orthorhombic SnS (JCPDS Card No. 39-0354). All of the recorded diffraction peaks in the XRD pattern of as-synthesized product can be well indexed to the diffractions from the corresponding crystallographic planes of orthorhombic SnS, except for the diffractions marked with *, which correspond to the diffractions from Sn foil (Figure S1 in the Supporting Information). This result indicates that the product is pure SnS in orthorhombic phase. It should be noted that the diffraction peaks at 32.0°, 44.8°, and 73.2° could embody the superposition of the diffractions of orthorhombic SnS and tetragonal Sn due to the overlap of the corresponding diffraction positions. Moreover, the sharp and strong diffraction peaks in the XRD pattern of the product imply that high crystallinity can be obtained at relatively low temperature (220 °C), which is important for semiconductor materials, since high crystallinity generally means less defects and high carrier mobility, and thus good performance in optoelectronic and photovoltaic applications.

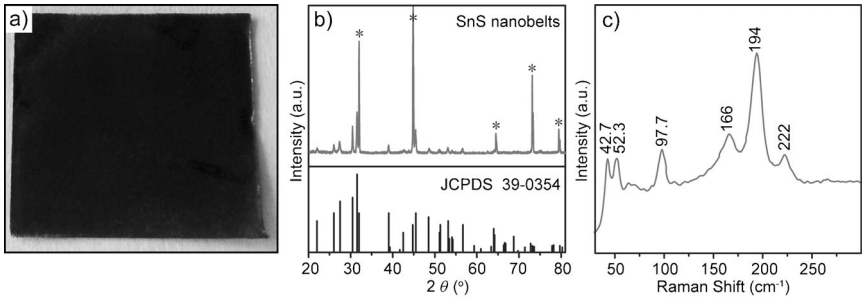

Figure 1. a) Optical photograph of the SnS nanostructured film. b) XRD patterns of SnS nanobelts and orthorhombic SnS (JCPDS Card No. 39-0354) as reference. c) Raman spectrum of SnS nanobelts.

In order to corroborate the composition of the product, the Raman spectrum was recorded, as shown in Figure 1c. The Raman vibration modes at 42.7, 52.3, 97.7, 166, 194, and 222 cm^{-1} are clearly distinguished in the spectrum. According to previous studies on Raman spectra of orthorhombic SnS, the observed Raman features at 42.7, 97.7, 194, 222 cm^{-1} can be assigned to the A_g modes of orthorhombic SnS, and those at 52.3 and 166 cm^{-1} can be attributed to its B_{3g} modes.[12] No additional Raman vibrations were observed in the spectrum. These results indicate that the product is composed of pure SnS in orthorhombic phase, which

is in good agreement with the XRD results. It is also noted that no obvious B_{1g} and B_{2g} modes were detected in the Raman spectrum, which suggests that the direction of the scattered beam could parallel to the *b* axis, probably due to a highly orientated arrangement of product.[12b]

The morphology and composition of the synthesized products were further characterized by scanning electron microscope (SEM) equipped with an energy-dispersive X-ray detector. As shown in Figure 2a, the typical SEM image indicates the products are composed of belt-like nanostructures with smooth outer surfaces and lengths of 1–2 μm, which grew directly on the substrate. The top-view SEM image (Figure 2b) shows the flat cross-section of the nanobelts with a width of about several tens to 150 nm and a thickness of 30–40 nm. Energy-dispersive X-ray spectrometry (EDS) results (Figure 2c) corroborate that all nanobelts contain only the elements Sn and S in a composition ratio of 57.3:42.7. The excessive Sn likely stems from unreacted tin metal underneath the SnS nanobelts, consistent with the XRD analysis.

The crystal structure of the nanobelts was investigated further by transmission electron microscopy (TEM) and high-resolution TEM (HRTEM). The low-magnification TEM image in Figure 2d shows that the nanobelt has smooth rectangular side surfaces. The ripple-like contrast difference on the nanobelt is typical of single-crystalline materials and is usually caused by the strain from bending and twisting the nanobelt.[7,13] EDS analysis on this nanobelt (Figure S2 in the Supporting Information) indicates that the atomic percentages of Sn and S in the nanobelt are 49.9% and 50.5%, respectively, thus giving clear evidence that the nanobelts are pure SnS. More details are revealed in the HRTEM image of part of the SnS nanobelt (Figure 2e). The clear and continuous lattice fringes without obvious detects over the whole area indicate single-crystalline nature and good crystallinity of the nanobelt. The distance of 0.294 nm and the angle of 92° between adjacent lattice fringes match well with the interplanar spacing and the interplanar angle of (101) planes and ($\bar{1}$01) planes of orthorhombic SnS, respectively. The distance of 0.200 nm between adjacent lattice fringes perpendicular to the length of the nanobelt corresponds to the (002) interplanar spacing of orthorhombic SnS, thus indicating that the nanobelt grew along the [002] crystallographic direction. The selected area electron diffraction (SAED) pattern (Figure 2f) taken directly on the region in Figure 2e presents a clear diffraction spot array, which corroborates the single-crystalline structure of the nanobelt. All diffraction spots can be indexed to the corresponding crystallographic planes of orthorhombic SnS.

It is well known that the morphology and size of nanostructures significantly influence device performance, especially for thin-film photovoltaic devices, since they rely on light absorption and carrier transportation. In order to demonstrate the controllability of monolithic SnS nanostructured films prepared using the simple solvothermal synthesis reported herein, a series of experiments was carried out by changing reaction conditions such as volume ratio of mixed solvents. It was found that the morphologies of SnS nanostructures are closely related to the volume ratio of the used mixed solvents (octanol/octylamine). Typical SEM images of the samples prepared at same conditions except for different volume ratios of octanol to octylamine are shown in Figure 3. XRD patterns show that all products are pure orthorhombic-phase SnS (Figure S4 in the Supporting Information). Short rod-like nanostructures with a diameter of about 100 nm were obtained when octylamine was used alone (Figure 3a). Low-magnification SEM images show that these rod-like nanostructures cover the whole foil (Figure S3a in the Supporting Information). When octanol (5 mL) was added to reach an octanol/octylamine ratio of 5:9, larger nanosheets with smooth surfaces and facets several micrometers wide and approximately 20 nm thick were achieved and coexisted with some nanorods (Figure 3b). Further increasing the amount of octanol to 7 mL (octanol/octylamine 1:1), SnS nanobelts 1–2 μm long, 100–150 nm wide, and approximately 20 nm thick dominated on the film (Figure 2a,b). As the amount of octanol was increased to 9 mL (octanol/octylamine 9:5), nanostructures tended to be rod-like again (Figure 3c). Lastly, when pure octanol was used as solvent, thin nanoflakes about 10 nm thick and several hundred nanometers wide formed in-

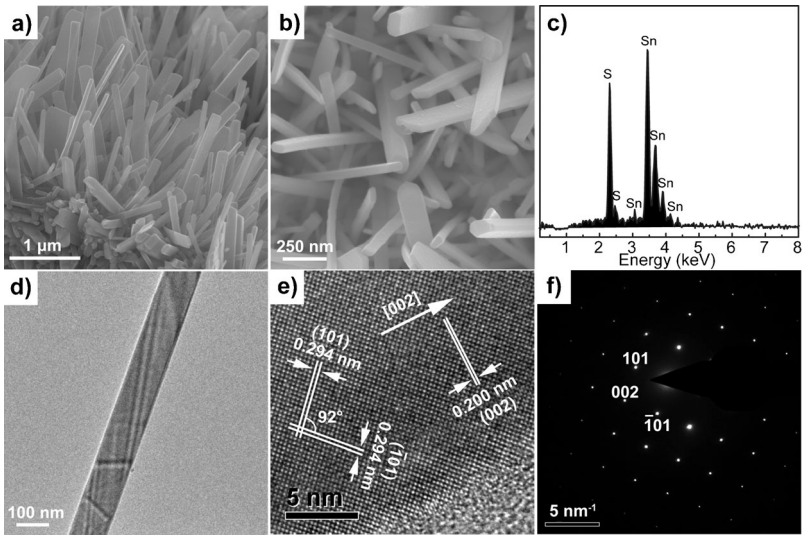

Figure 2. a) Side-view and b) top-view SEM images of nanobelts. c) EDS spectrum of SnS nanobelts. d) Low-magnification TEM image of a single SnS nanobelt. e) HRTEM image of a SnS nanobelt. f) SAED pattern directly taken on the region in (e).

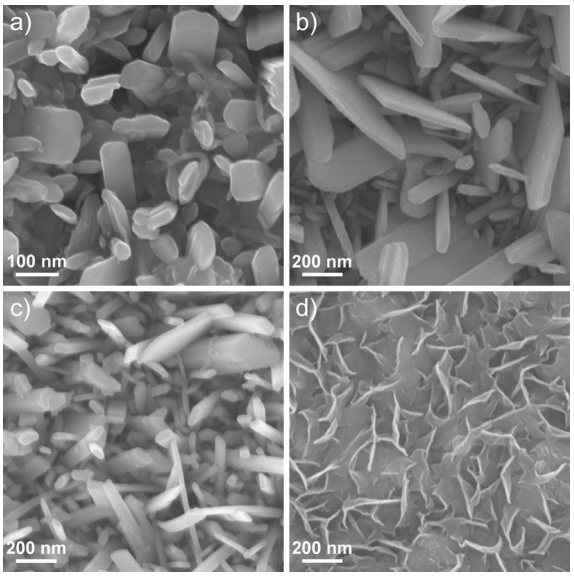

Figure 3. SEM images of SnS nanostructures obtained at different ratios of octanol/octylamine: a) 0:14, b) 5:9, c) 9:5, and d) 14:0.

stead (Figure 3d). It should be noted that similar nanostructures appeared on the whole foil in each case for a given solvent ratio, as indicated in the low-magnification SEM images (Figure S3 in Supporting Information), which means that the solvents played an important role in directing the formation of SnS nanostructures. Actually, some studies have reported that the coordinating effect and polarity of solvents significantly affected the morphologies of nanostructures.[14] Yadong Li and co-workers reported that metal powders and sulfur could be used as reactants to synthesize metal sulfide nanoparticles in ethylenediamine solution.[15] The ethylenediamine was claimed to not only produce active sulfur species in solution but also to play a role in the activation of the metal surface and the electron transfer in reactions. It was also reported that various sulfur imides (e.g. S_7NH) as well as sulfur nitrogen anions and sulfur polyanions (e.g. S_6^{2-}, S^{4-}, S_4N^-, S_7NH) could exist in sulfur–ammonia solution.[16] These species react with metallic tin and form tin sulfide. In the present study, tin foil and sulfur powder reacted in octylamine/octanol solution to produce tin(II) sulfide. It is believed that the coordinating effect and the selective adsorption of octylamine and octanol molecules on different crystallographic surfaces during the growth of SnS crystals could be responsible for the formation of 1D nanostructures, although the details need be further unveiled.

As encouraged by the belt-like morphology and good crystallinity of the synthesized SnS nanobelt, a photoelectric device and a field emission transistor (FET) based on single SnS nanobelts were fabricated to explore their potential in these applications. Figure 4a depicts a typical device based on a single SnS nanobelt. The details about device fabrication are given in Experimental Section. In brief, nanobelts were deposited onto the Si/SiO_2 substrate in proper density. The contacts on two ends of the single nanobelt were de-

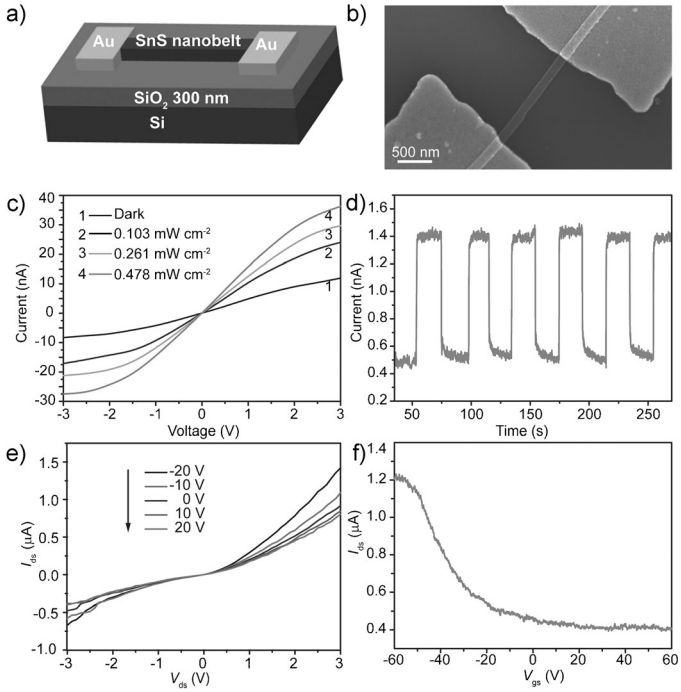

Figure 4. a) Schematic structure of device based on a single SnS nanobelt. b) SEM image of the measured FET device. The channel length between the two electrodes is 1.57 μm, and the width of the nanobelt is 140 nm. c) Dark current and photocurrents at different incident powder densities. d) Photoswitching behavior of a device based on a single SnS nanobelt with illumination of 0.478 mW cm^{-2} on and off at a bias voltage of 0.1 V. e) Typical curves of source–drain current (I_{ds}) as a function of source–drain voltage (V_{ds}) on the SnS nanobelt FET at different gate voltages (V_{gs}). f) I_{ds} vs. V_{gs} plot measured in the dark at $V_{ds}=2$ V on the same FET device shown in (b).

fined by electron-beam lithography, followed by the thermal deposition of Cr/Au. All photoresponse and FET measurements were carried out at room temperature in air. The current-voltage (I–V) characteristics of the device were recorded with a Keithley 4200 semiconductor characterization system in both dark and light conditions. Figure 4c presents typical I–V curves at varying incident light intensities of 0.103, 0.261, and 0.478 mW cm^{-2}. The recorded currents sharply increase even at very weak illumination compared to that in the dark, thus indicating the contribution from photogenerated carriers. For example, the current rises to 24 nA at an illumination of 0.103 mW cm^{-2} from 12 nA in the dark at a bias voltage of 3 V, which means the SnS nanobelt device is very sensitive to light. Moreover, it was found that the generated photocurrents depend on the power intensities of the illuminating light. Stronger illuminating light generates a larger photocurrent, which suggests that the photocurrent is mainly determined by the amount of photon-generated carriers under illumination. In order to show the reliability of the photoresponse from nanodevices based on single SnS nanobelts, the current curve as a function of time was recorded at a bias voltage of 0.1 V. As shown in Figure 4d, when the incident light was turned on and off, the nanodevice exhibited current in two distinct

states, an 'OFF' state at low current level in the dark and an 'ON' state at high current level under illumination. It can be seen that the current ramped to the 'ON' state at 1.4 nA from the 'OFF' state at 0.5 nA within tens of milliseconds when incident light of 0.478 mW cm^{-2} was on. The switching is fast and reversible, and the photocurrent is steady in the long term. These results demonstrated that SnS nanobelts showed good photoresponse and can be potentially used for photovoltaics.

The electron-transport properties of the SnS nanobelt were further investigated by FET measurement. Figure 4e plots the typical curves of source–drain current (I_{ds}) as a function of source–drain voltage (V_{ds}) at varying gate voltages (V_{gs}). When the gate voltage increases, I_{ds} decreases correspondingly, indicating the gate-dependent $I_{ds}-V_{ds}$ effect and the p-type conductivity of the device.[17] The gating behavior was further characterized by recording I_{ds} versus V_{gs} at constant $V_{ds}=2$ V (Figure 4f). It suggests that the source–drain current decreases with an increase in gate potential, thus indicating the typical p-type characteristics, that is, holes rather than electrons as carriers dominate inside the SnS nanobelt. In order to calculate the hole mobility in the SnS nanobelt, the transconductance $g_m=dI_{ds}/dV_{gs}$ of the device was determined by fitting the linear region of the I_{ds}–V_{gs} curve in Figure 4f. The channel length and width of the nanobelt device were measured based on the SEM image in Figure 4b. The field effect mobility for this device was calculated by Equation (1):[18]

$$\mu = L/(W \times C_{ox} \times V_{ds}) \times dI_{ds}/dV_{gs} \quad (1)$$

where C_{ox} is the capacitance per unit area between the conducting channel and the backgate ($C_{ox}=\varepsilon_o\varepsilon_r/d$; $\varepsilon_0=8.854\times10^{-12}$ F m^{-1}; ε_r for SiO_2 is 3.9, and d is the thickness of SiO_2 dielectric layer, ca. 300 nm), L is 1.57 μm; W is 0.14 μm; dI_{ds}/dV_g is -25.31 nA V^{-1} based on the slope in the linear region of the $I_{ds}-V_{gs}$ curve in Figure 4f; and V_{ds} is 2 V. As a result, the calculated hole mobility of the device is 12.33 cm^2 V^{-1} s^{-1}. Similar mobility values can be obtained on different single-nanobelt devices. This value is comparable to that of the state-of-the-art nanocrystals-based devices[19] and much higher than the reported mobility for a SnS nanoribbon device[3a] as well as PbS and PbTe nanowire FET devices where the nanowires are obtained by the chemical vapor transport method.[20] It is believed that the mobility of the present SnS nanobelt device could be further improved by either using HfO_2 as top gate and mobility booster[21] or by proper doping to increase its hole concentration.

Conclusions

In summary, monolithic SnS nanostructured films have been fabricated on tin foil substrate via a facile solution-based approach. It was found that the morphologies of nanostructured films could be tuned from well-defined orthorhombic SnS nanobelt arrays to nanorods, nanosheets, or nanoflakes by simply changing the ratio of solvents used. The photoelectric conversion and electron transport properties of the synthesized single-crystalline nanobelt have been investigated by fabricating the corresponding devices with single SnS nanobelts. It was shown that the SnS nanobelt exhibited a fast and reliable photoresponse even at an illumination intensity as weak as 0.103 mW cm^{-2}. Measurement on a SnS FET device also indicated that the synthesized SnS nanobelt demonstrated a hole mobility as high as 12.33 cm^2 V^{-1} s^{-1}. These results reveal that the reported approach for preparing monolithic SnS nanostructured films could be useful to explore potential applications in photovoltaics and electronics of SnS as a low-cost, earth-abundant, and environmentally friendly material.

Experimental Section

Materials

Tin foil, sulfur powder, octanol, and octylamine were purchased from Alfa Aesar and directly used without further purification. Deionized water with a resistivity of 18.2 MΩ cm^{-1} (Millipore) was used in all experiments.

Synthesis of SnS Nanobelt Films

Monolithic SnS nanobelt films were prepared by a simple solvothermal process by using tin foil and sulfur powder as starting materials with no addition of any surfactants or capping agents. In a typical procedure, a 1 cm × 1 cm piece of Sn foil (69.74 mg) was pretreated in 1 M HCl aqueous solution and then thoroughly washed with deionized water in an ultrasonic bath. The cleaned Sn foil was then put into a 25 mL Teflon-lined autoclave. Subsequently, sulfur powder (18.80 mg) was added to achieve a 1:1 molar ratio of Sn:S. Octylamine (7 mL) and octanol (7 mL) were typically filled into autoclave as solvents to prepared nanobelt films. Afterwards, the autoclave was kept at 220 °C for 12 h and then allowed cooled to ambient room temperature. The obtained foil with black substance on the surface was rinsed with ethanol and water and then dried in an oven at 60 °C for 2 h.

Characterization

The crystal structure of the product was determined by X-ray diffraction (XRD) using a Rigaku D/max2500 diffractometer with Cu Kα1 radiation ($\lambda=1.54056$ Å). The morphologies and composition of SnS nanostructures were investigated by scanning electron microscopy (SEM, Hitachi S-4800, Japan) with an energy-dispersive X-ray detector (Oxford Inc.) operating at 15 kV. Transmission electron microscopy (TEM) and high-resolution TEM (HRTEM) experiments were performed on a Tecnai G2 F20 U-TWIN instrument (FEI, USA) equipped with an energy-dispersive X-ray detector (EDAX Inc.) working at an accelerating voltage of 200 kV.

Fabrication of Single SnS Nanobelt Devices

SnS nanobelts were dispersed in ethanol and then deposited onto a highly doped Si substrate covered with 300 nm thick SiO_2 as the dielectric layer. Source and drain contacts to single SnS nanobelt were defined by electron-beam lithography on a PMMA950A4 resist (MicroChem Inc.) by using an SEM/FIB (focused ion beam) dual-beam instrument (Nova 200 NanoLab, FEI) interfaced with Elphy Quantum software (Raith Company), followed by the thermal evaporation of 5 nm Cr/90 nm Au. After lift-off of the resist in acetone, chips with SnS nanobelt FETs were rinsed thoroughly with acetone and isopropyl alcohol before blow-drying with N_2.

Electrical Measurements

Current–voltage (*I–V*) characteristics and FET electric measurements of the single SnS nanobelt devices were recorded with a Keithley 4200 semiconductor characterization system and a Micromanipulator 6150 probe station in a Faraday box at room temperature in air. An iodine–tungsten lamp was selected as the white light source. The incident light density was calibrated with an optical power meter.

Acknowledgements

This work was supported by the National Natural Science Foundation of China (Grants Nos. 91127044, 21173237, and 21121063), the National Key Project on Basic Research (Grants No. 2009CB930400 and 2011CB808700), and the Chinese Academy of Sciences.

[1] S. E. Habas, H. A. S. Platt, M. F. A. M. van Hest, D. S. Ginley, *Chem. Rev.* **2010**, *110*, 6571–6594.
[2] A. de Kergommeaux, J. Faure-Vincent, A. Pron, R. de Bettignies, B. Malaman, P. Reiss, *J. Am. Chem. Soc.* **2012**, *134*, 11659–11666.
[3] a) Z. Deng, D. Cao, J. He, S. Lin, S. M. Lindsay, Y. Liu, *ACS Nano* **2012**, *6*, 6197–6207; b) M. Sugiyama, K. T. R. Reddy, N. Revathi, Y. Shimamoto, Y. Murata, *Thin Solid Films* **2011**, *519*, 7429–7431; c) W. Albers, C. Haas, H. Vink, J. Wasscher, *J. Appl. Phys.* **1961**, *32*, 2220–2225.
[4] a) Y. Xu, N. Al-Salim, C. W. Bumby, R. D. Tilley, *J. Am. Chem. Soc.* **2009**, *131*, 15990–15991; b) W. Guo, Y. Shen, M. Wu, L. Wang, L. Wang, T. Ma, *Chem. Eur. J.* **2012**, *18*, 7862–7868.
[5] a) S. G. Hickey, C. Waurisch, B. Rellinghaus, A. Eychmuller, *J. Am. Chem. Soc.* **2008**, *130*, 14978–14980; b) J. J. Ning, K. K. Men, G. J. Xiao, L. Wang, Q. Q. Dai, B. Zou, B. B. Liu, G. T. Zou, *Nanoscale* **2010**, *2*, 1699–1703; c) Z. Deng, D. Han, Y. Liu, *Nanoscale* **2011**, *3*, 4346–4351.
[6] a) J. Chao, Z. Wang, X. Xu, Q. Xiang, W. Song, G. Chen, J. Hu, D. Chen, *RSC Adv.* **2013**, *3*, 2746–2753; b) S. K. Panda, A. Datta, A. Dev, S. Gorai, S. Chaudhuri, *Cryst. Growth Des.* **2006**, *6*, 2177–2181.
[7] Y. Zhang, J. Lu, S. Shen, H. Xu, Q. Wang, *Chem. Commun.* **2011**, *47*, 5226–5228.
[8] a) D. Avellaneda, G. Delgado, M. T. S. Nair, P. K. Nair, *Thin Solid Films* **2007**, *515*, 5771–5776; b) A. Stavrinadis, J. M. Smith, C. A. Cattley, A. G. Cook, P. S. Grant, A. A. R. Watt, *Nanotechnology* **2010**, *21*, 185202.
[9] a) J. Zhu, C. M. Hsu, Z. F. Yu, S. H. Fan, Y. Cui, *Nano Lett.* **2010**, *10*, 1979–1984; b) M. G. Deceglie, V. E. Ferry, A. P. Alivisatos, H. A. Atwater, *Nano Lett.* **2012**, *12*, 2894–2900; c) S. F. Leung, M. Yu, Q. F. Lin, K. Kwon, K. L. Ching, L. L. Gu, K. Yu, Z. Y. Fan, *Nano Lett.* **2012**, *12*, 3682–3689; d) D. Liang, Y. J. Huo, Y. Kang, K. X. Wang, A. J. Gu, M. Y. Tan, Z. F. Yu, S. Li, J. Y. Jia, X. Y. Bao, S. Wang, Y. Yao, H. S. P. Wong, S. H. Fan, Y. Cui, J. S. Harris, *Adv. Energy Mater.* **2012**, *2*, 1254–1260.
[10] a) E. Garnett, P. D. Yang, *Nano Lett.* **2010**, *10*, 1082–1087; b) T. J. Kempa, R. W. Day, S. K. Kim, H. G. Park, C. M. Lieber, *Energy Environ. Sci.* **2013**, *6*, 719–733; c) S. W. Boettcher, J. M. Spurgeon, M. C. Putnam, E. L. Warren, D. B. Turner-Evans, M. D. Kelzenberg, J. R. Maiolo, H. A. Atwater, N. S. Lewis, *Science* **2010**, *327*, 185–187; d) M. D. Kelzenberg, S. W. Boettcher, J. A. Petykiewicz, D. B. Turner-Evans, M. C. Putnam, E. L. Warren, J. M. Spurgeon, R. M. Briggs, N. S. Lewis, H. A. Atwater, *Nat. Mater.* **2010**, *9*, 239–244.
[11] J. Liu, D. Xue, *Electrochim. Acta* **2010**, *56*, 243–250.
[12] a) S. Sohila, M. Rajalakshmi, C. Ghosh, A. K. Arora, C. Muthamizhchelvan, *J. Alloys Compd.* **2011**, *509*, 5843–5847; b) H. Chandrasekhar, R. Humphreys, U. Zwick, M. Cardona, *Phys. Rev. B* **1977**, *15*, 2177–2183.
[13] a) Z. W. Pan, Z. R. Dai, Z. L. Wang, *Science* **2001**, *291*, 1947–1949; b) P. X. Gao, Y. Ding, W. J. Mai, W. L. Hughes, C. S. Lao, Z. L. Wang, *Science* **2005**, *309*, 1700–1704.
[14] a) H. L. Zhu, D. R. Yang, Y. J. Ji, H. Zhang, X. F. Shen, *J. Mater. Sci.* **2005**, *40*, 591–595; b) A. Cao, J. Hu, L. Wan, *Sci. China Chem.* **2012**, *55*, 2249–2256; c) C. H. An, K. B. Tang, G. Z. Shen, C. R. Wang, Q. Yang, B. Hai, Y. T. Qian, *J. Cryst. Growth* **2002**, *244*, 333–338; d) Y. Li, Y. Ding, H. Liao, Y. Qian, *J. Phys. Chem. Solids* **1999**, *60*, 965–968; e) Y. Yin, S. Xin, L. Wan, C. Li, Y. Guo, *Sci. China Chem.* **2012**, *55*, 1314–1318; f) C. Zhang, K. Li, S. Song, D. Xue, *Chem. Eur. J.* **2013**, *19*, 6329–6333; g) K. Li, M. Li, D. Xue, *J. Phys. Chem. A* **2012**, *116*, 4192–4198.
[15] Y. D. Li, Z. Y. Wang, Y. Ding, *Inorg. Chem.* **1999**, *38*, 4737–4740.
[16] G. Henshaw, I. P. Parkin, G. A. Shaw, *J. Chem. Soc. Dalton Trans.* **1997**, 231–236.
[17] a) G. Shen, J. Xu, X. Wang, H. Huang, D. Chen, *Adv. Mater.* **2011**, *23*, 771–775; b) G. Shen, B. Liang, X. Wang, H. Huang, D. Chen, Z. L. Wang, *ACS Nano* **2011**, *5*, 6148–6155.
[18] Z. Yin, H. Li, H. Li, L. Jiang, Y. Shi, Y. Sun, G. Lu, Q. Zhang, X. Chen, H. Zhang, *ACS Nano* **2012**, *6*, 74–80.
[19] a) D. V. Talapin, J.-S. Lee, M. V. Kovalenko, E. V. Shevchenko, *Chem. Rev.* **2010**, *110*, 389; b) J.-S. Lee, M. V. Kovalenko, J. Huang, D. S. Chung, D. V. Talapin, *Nat. Nanotechnol.* **2011**, *6*, 348–352; c) D. J. Late, B. Liu, H. R. Matte, V. P. Dravid, C. Rao, *ACS Nano* **2012**, *6*, 5635–5641; d) D. S. Chung, J.-S. Lee, J. Huang, A. Nag, S. Ithurria, D. V. Talapin, *Nano Lett.* **2012**, *12*, 1813–1820.
[20] M. Fardy, A. I. Hochbaum, J. Goldberger, M. M. Zhang, P. Yang, *Adv. Mater.* **2007**, *19*, 3047–3051.
[21] B. Radisavljevic, A. Radenovic, J. Brivio, V. Giacometti, A. Kis, *Nat. Nanotechnol.* **2011**, *6*, 147–150.

Received: May 3, 2013
Revised: May 31, 2013
Published online: July 11, 2013

